PNAS RESEARCH ARTICLE | MICROBIOLOGY OPEN ACCESS

Reprogrammed SimCells for antimicrobial therapy

Yun Dong[a], Xianglin Ji[b], Tao Dong[c], Yun Wang[b], Erik Bakkeren[d,e], Kevin R. Foster[d], and Wei E. Huang[a,1]

Affiliations are included on p. 11.

Edited by Ralph R. Isberg, Tufts University School of Medicine, Boston, MA; received June 28, 2025; accepted February 18, 2026

Antimicrobial resistance (AMR) is a critical global health challenge. In this study, we developed a platform based on chromosome-free and nonreplicating simple cells (SimCells, size 1 to 2 μm) and mini-SimCells (size 100 to 400 nm) for targeted pathogen elimination. Engineered with surface-displayed nanobodies, SimCells and mini-SimCells selectively bind bacteria expressing specific antigens (e.g., OmpA in *Escherichia coli*). The selective interactions facilitate close SimCell-pathogen proximity, enabling two antimicrobial mechanisms: direct injection of toxic effectors into bacterial cytoplasm via a heterologous expression of type VI secretion system (T6SS), and enzymatic conversion of aspirin into catechol by engineered salicylate hydroxylase, leading to sustained local production of hydrogen peroxide (H_2O_2). Our results demonstrate that both reprogrammed SimCells and mini-SimCells can eliminate target *E. coli* with high specificity and efficiency. Multidose reprogrammed mini-SimCell treatment led to a 10^3-fold selective reduction of targeted bacteria in mixed microbial communities, with minimal disruption to nontarget bacteria. We demonstrate that reprogrammed mini-SimCells, engineered with nanobody targeting outer membrane protein OmpA of the clinically relevant multidrug-resistant pathogen *E. coli* ST131, achieved elimination efficiencies over 97% at 24 and 48 h. This modularized "plug-and-play" antimicrobial platform provides a highly specific, efficient, and adaptable solution for combating diverse AMR pathogens.

synthetic biology | SimCells | nanobody | AMR | therapy

Significance

Antimicrobial-resistant (AMR) bacteria cause millions of deaths worldwide annually, representing a critical global health challenge. In this study, we developed a therapeutic platform using two types of chromosome-free, nonreplicating engineered bacterial cells: SimCells (1 to 2 μm) and mini-SimCells (100 to 400 nm). These SimCells were engineered to selectively bind to targeted *Escherichia coli*, facilitating precise delivery of toxic proteins via a Type VI secretion system (T6SS) and localized generation of hydrogen peroxide from aspirin. We demonstrate that mini-SimCells eliminated over 97% of a targeted AMR strain within 48 h. Moreover, multiple-dose administration achieved a selective 10^3-fold reduction of targeted *E. coli* in mixed microbial communities. This modular "plug-and-play" platform offers an adaptable solution against diverse multidrug-resistant pathogens.

Antimicrobial resistance (AMR) is one of the top global public health challenges facing humanity by the World Health Organization (WHO) (1, 2). Predicted to become the next worldwide pandemic, AMR could cause over 10 million deaths annually and 100 trillion dollars of global GDP loss cumulatively by 2050 (3–6). Despite this urgency, the discovery of new antibiotics has stagnated. The last new class of antibiotics was discovered in the 1980s (7, 8), with only recent reports in 2024 announcing a promising new antibiotic, zosurabalpin (9). Significant advancements in chemical synthesis (10, 11), high-throughput screening (12–14), rational design (15–17), and particularly AI (18–23), have provided new pipeline for new antibiotic discovery. However, the antibiotic discovery might be insufficient compared to the rapid pace and spread of AMR. It is alarming that AMR has been developed for every approved antibiotic class currently being launched (24). The development of alternative antimicrobial strategies has been promoted, including therapies based on bacteriophage (25–27), monoclonal antibodies (28–30), and antibacterial peptides (31–33). However, these approaches face limitations such as stability issues, potential toxicity, and high manufacturing costs (33–35) (*SI Appendix*, Table S1).

Advancements in synthetic biology have led to the design of genetically engineered live microorganisms for the treatment or prevention of AMR pathogens in humans (36). Various microbial genetic components and tools have promoted the development of live biotherapeutic products (LBPs), providing a promising approach to address metabolic disorders, cancer therapy, and other unmet clinical needs (37, 38). However, biocontainment and biosafety concerns still restrain bacterial therapeutics from reaching a high public acceptability (39). To mitigate safety concerns, probiotic strains such as *Lactococcus lactis* (40)and *Escherichia coli* Nissle 1917 (EcN) (41, 42) have been used as chassis for therapy. Alternatively, attenuated strains with native tropism or colonizing features, such as *Listeria* (43) and *Salmonella* (44, 45), are also employed. Despite the selection of the safety profile of the chassis, the risk of uncontrolled replication remains a challenge. A few strategies, such as conditional kill switches (46) and auxotrophy (47), have been used to prevent engineered bacteria from proliferating uncontrollably within or outside the human body and from escaping into the environment. Although these measurements restrict growth, concerns persist about the evolutionary stability of the introduced genetic modification and the potential risk of horizontal gene transfer (HGT).

To address these challenges associated with bacterial AMR, we developed customizable platforms based on SimCells (simple cell) (48) and mini-SimCells (49, 50) for use in antimicrobial therapy. SimCells and mini-SimCells are chromosome-free, nonreplicating, and

Author contributions: W.E.H. designed research; Y.D., X.J., Y.W., and E.B. performed research; T.D. and K.R.F. contributed new reagents/analytic tools; Y.D. X.J., and W.E.H. analyzed data; and Y.D. and W.E.H. wrote the paper.

Competing interest statement: Y.D. and W.E.H. have filed a provisional patent application with the UK Patent Office related to this work.

This article is a PNAS Direct Submission.

[1]To whom correspondence may be addressed. Email: wei.huang@eng.ox.ac.uk.

This article contains supporting information online at https://www.pnas.org/lookup/suppl/doi:10.1073/pnas.2517118123/-/DCSupplemental.

Published March 17, 2026.

reprogrammable bacterial chassis that function as "smart" bioparticles (49, 51). SimCells (size 1 to 2 μm) are produced by removing native chromosomes using tightly controlled specific endonuclease and nuclease (48, 52). Mini-SimCells (size 100 to 400 nm) are generated through asymmetric division of bacteria with a *minD* gene deletion (53–55). Both SimCells and mini-SimCells can be produced from various bacteria strains (48, 56) and engineered to carry designed DNA for predefined functions (49–51) In this study, *E. coli* BL21 (DE3) and its ΔminD mutant were used as the chassis to generate SimCells and mini-SimCells, respectively. Both SimCells and mini-SimCells cannot replicate but retain the machinery of cells (e.g. transcription and translation). They are highly controllable and easy to produce from engineered parental bacterial cells (49, 50) In this study, the escape frequency of SimCells is below 10^{-8}, meeting the criteria of the NIH guidelines for clinical recombinant microorganisms (53). Mini-SimCells are essentially engineered minicells containing designed DNA. Clinical therapy based on minicells has been validated in both dogs and humans (phase I clinical trial), showing significant promise in safety and efficacy (54). Remarkably, minicell-based therapy has recently been granted "Fast-Track" status by the FDA (57). Hence, SimCell and mini-SimCell platforms not only meet safety standards but also show great potential in clinical applications, such as pathogen and cancer treatment (49, 51, 54, 58, 59).

Our strategy for antimicrobial therapy is engineering SimCells and mini-SimCells as smart "bioparticles" to selectively eradicate pathogens, while sparing nontarget bacteria (Fig. 1*A*). We engineered surface-displayed nanobodies on the outer membrane of SimCells and mini-SimCells using a modular surface display system (60), enabling selective recognition and binding to antigens on target pathogens. This nanobody–antigen interaction not only increases specificity, but also enhances antimicrobial effects that rely on close cell–cell proximity (Fig. 1*A*). Such mechanisms include "nano-needle" killing via type VI secretion system (T6SS) (61, 62) and localized release of high dose of antimicrobial compounds. Specifically, SimCells and mini-SimCells engineered with a modularized T6SS are supposed to deliver toxic effectors (63) to the cytoplasm of other bacteria in a contact-dependent manner (64–66). Another mechanism is to locally generate a high concentration of H_2O_2 via catalysis of aspirin by NahG salicylate hydroxylase enzyme (67–71).

In this study, we engineered a customizable SimCell and mini-SimCell platform that combined both mechanisms to deliver both rapid and sustained antimicrobial activity. Antimicrobial efficacy is significantly enhanced by the specific binding of SimCells and mini-SimCells to target bacteria via nanobody–antigen interactions, enabling immediate T6SS-mediated cytotoxicity followed by prolonged hydrogen-peroxide release. For proof of concept, a single safe dose of mini-SimCells killed 94% of the target bacteria within 24 h, and 99% after 48 h. In mixed microbial communities, four sequential doses achieved a 10^3-fold reduction of the target bacteria while leaving nontarget species largely unaffected. Engineered with native-antigen targeting nanobody, reprogrammed dual mechanism mini-SimCells successfully eliminated 97% of the target multidrug-resistant pathogen, *E. coli* ST131, within 24 h. These findings highlight the potential of SimCells and mini-SimCells for antimicrobial therapy and set a foundation for the development of clinically safe, custom-designable biotherapeutics to combat the escalating threat of antimicrobial resistance.

Results

Surface-Displayed Nanobody in *E. coli* Enables Selective Binding. First, the nanobodies and T6SS were characterized with the parental chassis strains before moving on to preparing SimCells

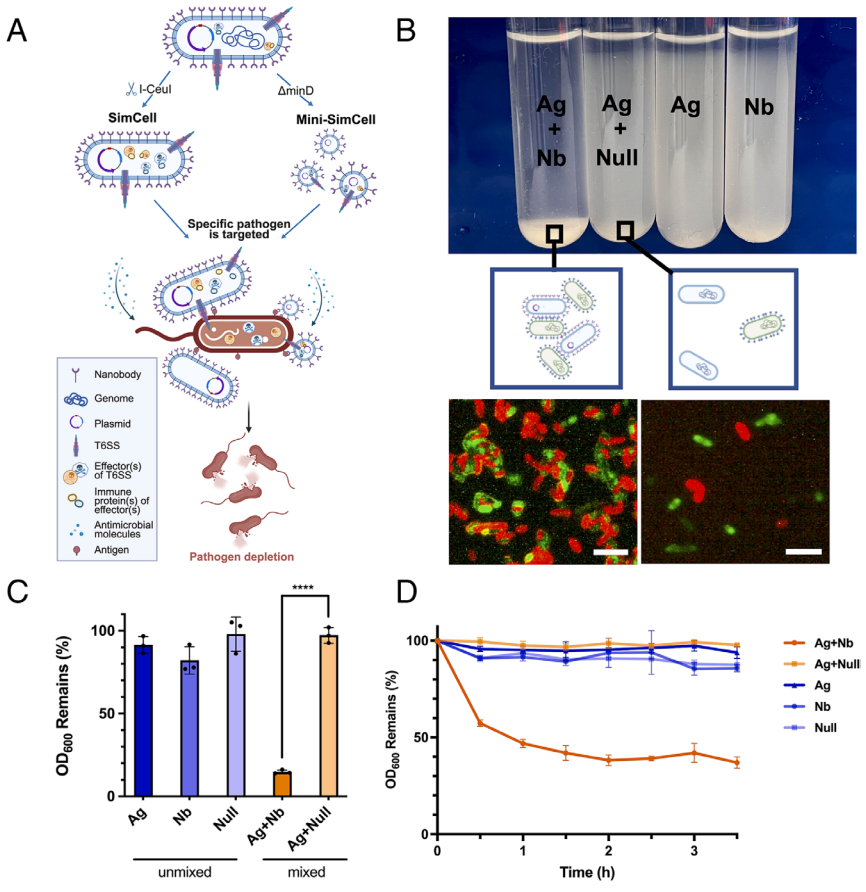

Fig. 1. Surface-displayed nanobody in engineered *E. coli* enables selective cell–cell binding via nanobody–antigen interactions. (*A*) Design of the SimCell and mini-SimCell platform for treating bacterial AMR. Surface-displayed nanobodies are engineered to the outer membrane of SimCell and mini-SimCell using a modular surface display system, to enable antigen recognition and selectively binding to target pathogens. This nanobody–antigen binding is expected to increase the specificity, shorten the distance, and enhance the efficiency of contact-dependent or enhanced inhibition mechanisms including toxic effector protein delivery through modularized T6SS and localized antimicrobial molecules generation. (*B*) Binding of Ag and Nb cells in a 1:1 ratio leads to both detectable macroscopic and microscopic aggregation compared to unmixed and nonadhesion (Ag+Null) conditions. Red: mRFP-labeled Nb/Null cells. Green: sfGFP-labeled Ag cells. (Scale bar, 10 μm.) (*C*) Ag–Nb aggregating cell mixture shows significant settling compared to unmixed and nonadhesion (Ag-Null) conditions after 12 h. (*D*) Time courses of macroscopic aggregation show significant settling within ~30 min. All cell cultures were mixed at time 0 and allowed to settle. OD_{600} from top 25% supernatant was continuously measured every 30 min for 3.5 h. For (*C* and *D*), all cultures were normalized to the same initial OD_{600} and mixed in 1:1 v/v ratio. n = 3 replicates, Error bars, ±1 SD, ****$P < 0.0001$ according to a 2-tailed paired *t* test.

and mini-SimCells. *E. coli* BL21(DE3) and its ΔminD mutant were used as the chassis to produce both SimCells and mini-SimCells. The smooth surface without flagella and fimbriae of the B lineage of *E. coli* BL21(DE3) minimizes interference with the nanobody–antigen interactions. It has been previously reported that an N terminus-fusion modular system can display nanobodies on the cell's outer membrane with precise folding and efficient localization (60). As a proof of concept, we employed a well-characterized antigen-nanobody pair, EPEA (Ag), and anti-EPEA (Nb) (72), to demonstrate the target-specific antimicrobial effect of SimCell therapy.

Surface-displayed nanobody expression and its antigen binding were verified at both macroscopic and microscopic levels. Strains expressing either antigen (Ag) or nanobody (Nb), as well as a null strain, were induced overnight with 100 ng/mL anhydrotetracycline (ATc), and labeled with superfolder GFP (sfGFP) (green) and mRFP (red), respectively. Stationary-phase cultures were normalized to the same optical density (OD_{600}), then left unmixed or mixed in a 1:1 ratio (Ag+Nb and Ag+Null, with the latter as a control without adhesion construct). After 12 h standing still, significant cell–cell aggregation was observed in cultures with adhesion pairs, while no such phenomena were seen in unmixed or control groups (Fig. 1*B*). From these, 10 μL cultures were collected from the bottom of both adhesion and nonadhesion groups, and performed the same dilution until single cells were loosely distributed in most views under the fluorescent microscope. Cells with adhesion pairs formed mesh-like-pattern aggregates (Fig. 1*B*). The aggregation was then quantified by measuring the OD_{600} from the upper 25% portion of the cultures (*SI Appendix*, Fig. S1*A*). A significant OD_{600} reduction (>85%) occurred for the adhesion group (Ag+Nb) (Fig. 1*C*). In the time-course experiment, supernatant density was measured every 30 min for 3.5 h. The OD_{600} reduced by more than 50% for the adhesion group within 1 h (Fig. 1*D*), indicating that Ag–Nb binding interaction is a rapid process.

The results suggest that the anti-EPEA Nb should be correctly folded and surface-displayed on the parental chassis strains. To further test nanobody stability, Nb-expressing strains were stored at either room temperature (RT), 20 °C, or 4 °C for 1, 5, and 10 d, then mixed with Ag-expressing *E. coli*, and macroscopic aggregation was monitored for 3 h (*SI Appendix*, Fig. S1*A*). There were no significant cell pellets observed in all the unmixed groups, indicating cell integrity and stability. Despite the extended time required to attain comparable aggregation intensity, nanobody activity was preserved in cells stored at both temperatures after 10 d (*SI Appendix*, Fig. S1*B*).

Nanobody–Antigen Pairs Enable Selective T6SS Killing of Target Cells. A plasmid containing complete gene cluster encoding T6SS from *Aeromonas dhakensis* (63), has been introduced to parental chassis strains (*SI Appendix*, Table S2). The plasmid contains a sfGFP-fused T6SS gene cluster controlled by either a native constitutive promoter (pT6S_NP) or a tetracycline-inducible promoter (pT6S_Tet), as well as inactive controls (pT6S_N3-NP and pT6S_N3-Tet), which contain a noncontractile 3-amino acid insertion in the subunits forming contractile outer sheath. The T6SS gene cluster encodes two effector-immunity paired proteins: a self-cleaving Rhs-family nuclease effector TseI with its cognate immunity protein TsiI (73), and a lysozyme effector TseP with its cognate immunity protein TsiP (74). Fluorescence microscopy analysis demonstrated the formation of contractile tubular structures, confirming T6SS activity (Fig. 2*A*). *E. coli* BL21(DE3) engineered with T6SS also proved a significant killing effect in contact-promoted (solid) condition (*SI Appendix*, Fig. S2*A*), confirming T6SS activity. Over 97% of constitutive T6SS-expressing cells exhibited active sfGFP after 96-h (*SI Appendix*, Fig. S2*B*) and maintained significant out-competitive capability against the prey cells (*SI Appendix*, Fig. S2*C*). These results indicate stable and robust expression of the T6SS across the cell population.

As the function of T6SS requires close cell–cell proximity and sustained interactions (75), we hypothesized that nanobody-mediated selective binding could promote $T6SS^+$ attacker cells to efficiently kill the targeted prey cells in a mixed population. *SI Appendix*, Fig. S3*A* shows that Nb–Ag interaction enhanced T6SS-mediated killing in solid conditions. In comparison to the contact-promoting killing on the solid surface, well-mixed suspension conditions are representative of clinical scenarios with planktonic pathogens. The results demonstrate that in a fluid environment, the attacker cells with both nanobody and active T6SS have a significant killing effect, with more than 84% of prey cells eliminated compared to the negative control group. However, the attacker cells with active T6SS ($T6SS^+$) without nanobodies were unable to eliminate prey cells (Fig. 2*B*). Interestingly, an inhibitory effect was also observed in the Nb-binding-only group (Fig. 2*B*), which may be attributed to the disruption of carbon-source uptake, motility, and membrane integrity in prey cells due to cell–cell aggregation (76). The synergistic functionality of both binding and $T6SS^+$ was markedly more pronounced. In the time-course experiment, a significant inhibition effect was detected within 4 h and continued to increase over time (Fig. 2*C*).

To verify that the surviving prey cells had not acquired resistance to T6SS-mediated killing, we tested various multiplicities of infection (MOI). Increased killing efficiency was observed with higher MOI, suggesting that the inability to eliminate 100% of the prey cells could be due to exhaustion of T6SS activity rather than prey resistance (*SI Appendix*, Fig. S3*B*). This limitation could potentially be addressed by increasing the attacker-to-prey ratio, regeneration of T6SS activity or administering multiple doses.

To evaluate whether the nanobody display confers target specificity to $T6SS^+$ attacker cells, we cocultured the attacker cells with a mixed prey population of Ag-positive *E. coli* BL21 (Ag^+) and Ag-negative *E. coli* DH10B (Ag^-). Selective killing should occur only when i) the nanobody matched the paired antigen and ii) attacker cells possessed an active T6SS. After 6 h of coincubation, more than 50% of Ag^+ cells were eliminated, whereas the Ag^- population showed no significant loss (Fig. 2*D* and *SI Appendix*, Fig. S3*C*). The results confirm that nanobody–antigen interactions enabled precise and T6SS-dependent elimination of the targeted prey bacteria, while sparing nontarget bacteria in a mixed microbial community.

T6SS Mediated Bacterial Killing in Reprogrammed SimCells. Building on the demonstrated nanobody–antigen specificity and T6SS-mediated killing, we next generated SimCells from our chassis strains. We previously reported the development and characterization of SimCells as a safe, reprogrammable, and customizable chassis for synthetic biology (48), especially beneficial for biomedical applications such as cancer therapy (49). The chromosome-free SimCells were produced by DNA cleavage at a conserved 19-bp recognition sequence (contained within a 26-bp fragment) in the 23S rRNA subunit using inducible expression of I-CeuI endonuclease, after which the bacterial native nuclease RecBCD initiated chromosomal degradation (52). Plasmids containing the I-CeuI endonuclease, the surface-displayed nanobody, and the T6SS machinery were introduced into the *E. coli* BL21 (DE3) chassis to produce and reprogram SimCells (*SI Appendix*, Table S2). Results from growth arrest assay (*SI Appendix*, Fig. S4*A*), DNA staining assay (*SI Appendix*,

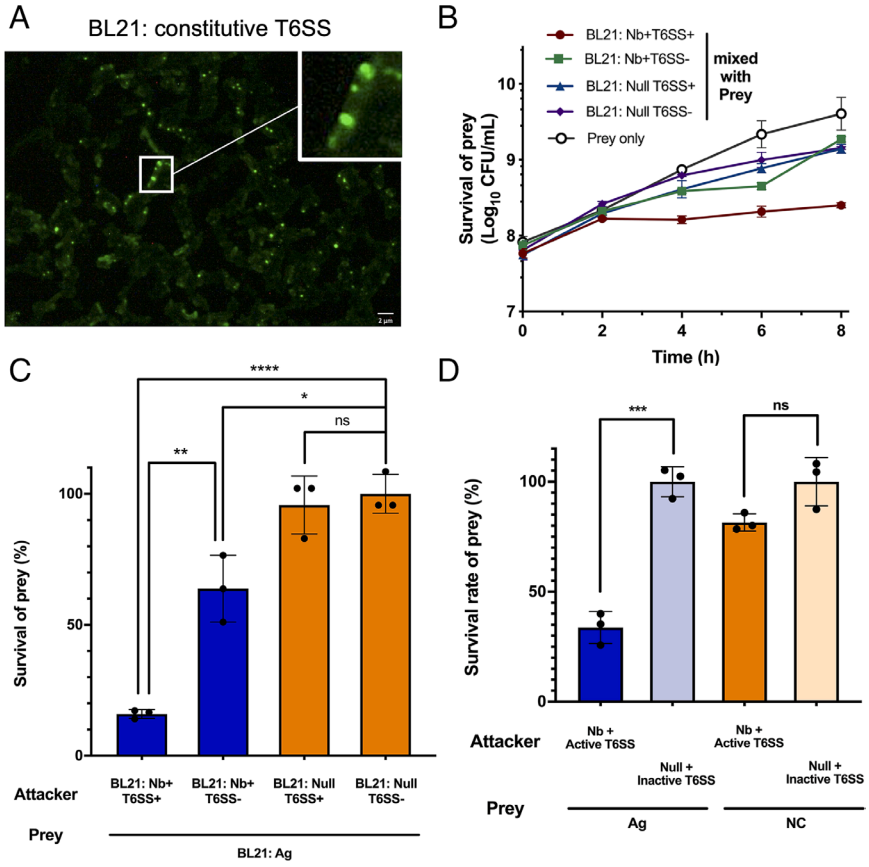

Fig. 2. Nanobody–antigen mediated cell–cell adhesion enables selectively depletion of target cells via T6SS in liquid condition. (*A*) Fluorescence microscopic analysis confirms the assembly of T6SS in laboratory *E. coli* strain BL21(DE3). C-terminal sfGFP was fused to VipA for labeling. Localized fluorescence signals were observed. Scale bar, 2 μm. (*B*) Nanobody–antigen binding enables an efficient T6SS-mediated killing in liquid condition. Incubation time = 6 h. Attacker: prey v/v ratio = 10:1. In schematic, target cells with surface antigen and programmed attacker cells (Nb+T6SS+/ Nb+T6SS-/Null T6SS+/Null T6SS−) are represented. Nb+ = cells with surface-displayed nanobody, Null = cells with no-adhesin. T6SS+ = cells with active induced T6SS, T6SS− = cells with inactive induced T6SS. (*C*) Time courses of nanobody-enhanced T6SS killing effect. Significant killing was observed after 2 h. Incubation time = 0,2,4,6,8 h. Attacker: prey v/v ratio = 10:1. (*D*) Nb–Ag recognition enables a specific T6SS-mediated killing in liquid condition. In schematic, programmed attacker cells (Nb+T6SS+) and Prey 1(Ag), Ag-expressed *E. coli* BL21, prey 2(NC), *E. coli* DH10B are represented. Incubation time = 6 h. Attacker: prey 1: prey 2 v/v ratio = 10:1:1. For (*B* to *D*), all cultures were normalized to the same initial OD_{600}. n = 3 replicates, Error bars, ±1 SD, $*P < 0.1$, $**P < 0.01$, $***P < 0.001$, $****P < 0.0001$ according to a 2-tailed paired *t* test. Survival rate was calculated as survival cells/ total prey cells.

Fig. S4*B*), and single-cell Raman spectra analysis (*SI Appendix*, Fig. S4*C*) collectively confirm that the resulting SimCells had high purity, with an escape frequency of less than 10^{-8} (*SI Appendix*, Fig. S4*D*), meeting the criteria of NIH guidelines for recombinant microorganisms (77).

We then assessed the binding ability and T6SS activity of the reprogrammed SimCells. The expression of both the nanobody and T6SS was induced prior to SimCell conversion to ensure the engineered proteins were fully assembled for operation. As shown in *SI Appendix*, Fig. S1*C*, significant macroscopic aggregation and OD_{600} reduction (>60%) were detected for the adhesion group (Ag+Nb-SimCell) after 3 h standing. Subsequent fluorescence analysis verified T6SS assembly (*SI Appendix*, Fig. S5*A*) and significant killing effect in solid condition suggested T6SS activity (*SI Appendix*, Fig. S5*B*) in our reprogrammed SimCells.

To validate nanobody-mediated, T6SS-dependent killing by SimCells, we cocultured antigen-positive (Ag^+) prey with attacker SimCells carrying different combinations of nanobody (Nb^+ or Nb^-) and T6SS ($T6SS^+$ or $T6SS^-$). After 6 h in minimal medium, Nb^+T6SS^+ SimCells eliminated more than 85 % of Ag^+ cells. In contrast, prey survival was roughly 50 % with nanobody binding alone (Nb^+T6SS^-), and moderate inhibition was observed with nonbinding $T6SS^+$ SimCells (Nb^-T6SS^+) (*SI Appendix*, Fig. S5*C*). These results confirm that SimCells retain measurable T6SS activity in suspension and demonstrate that specific nanobody binding is critical for maximizing T6SS-mediated killing in liquid culture.

T6SS Mediated Killing in Reprogrammed Mini-SimCells. Following validation of the nanobody-directed specific T6SS killing in SimCells, we subsequently established design feasibility in the mini-SimCell platform. Reprogrammed mini-SimCells were generated from the aberrant cell division of the ΔminD mutant of engineered parental cells. The *E. coli* BL21(DE3) ΔminD strain was previously developed and verified in our lab (49). Mini-SimCells were purified by gradient centrifugation to separate them from parental cells. The formation of $T6SS^+$ mini-SimCells was confirmed using a fluorescence microscope (Fig. 3*A*) and scanning electron microscope (SEM) (Fig. 3*B*). In addition, ZetaView analysis was used to characterize the size distribution of the mini-SimCells, where mini-SimCells with T6SS (T6SS mini-SimCells) were identified by sfGFP-labeling. Approximately 91% of mini-SimCells derived from parental cells (BL21 mini-SimCells) fell within the 100-300 nm size range, while over 33% of the Nb- and T6SS-expressing mini-SimCells (T6SS mini-SimCells) were larger than 300 nm (Fig. 3*C*). This finding was consistent with the SEM results, suggesting T6SS mini-SimCells were measured larger, likely due to the surface display of Nb and the assembly of the T6SS machinery, as the tail length of the T6SS "nano-needle" is dictated by the size of the bacterial cell (78). ZetaView concentration analysis of the mini-SimCells revealed approximately 2.20×10^{10} T6SS mini-SimCells within a total population of 3.56×10^{11} reprogrammed mini-SimCells purified from the original 100 mL culture (Fig. 3*C*). This represents a high production yield, indicating promising potential for future large-scale manufacturing applications.

T6SS activity in mini-SimCells was verified on solid media (*SI Appendix*, Fig. S6*A*), and nanobodies enabled the T6SS to efficiently kill prey cells also in liquid media. We tested the limit of killing (LOK) for Nb-T6SS mini-SimCells using a dose of 1×10^{10} Nb-T6SS mini-SimCells, which has been approved as safe in previous human trials (79). Experiments were conducted at MOI of 62.5, 100, 500, 2,500, 5,000, and 10,000. As shown in *SI Appendix*, Fig. S6*B*, significant inhibition was observed across all groups, with a marked increase in killing efficiency at higher MOI. By fitting an

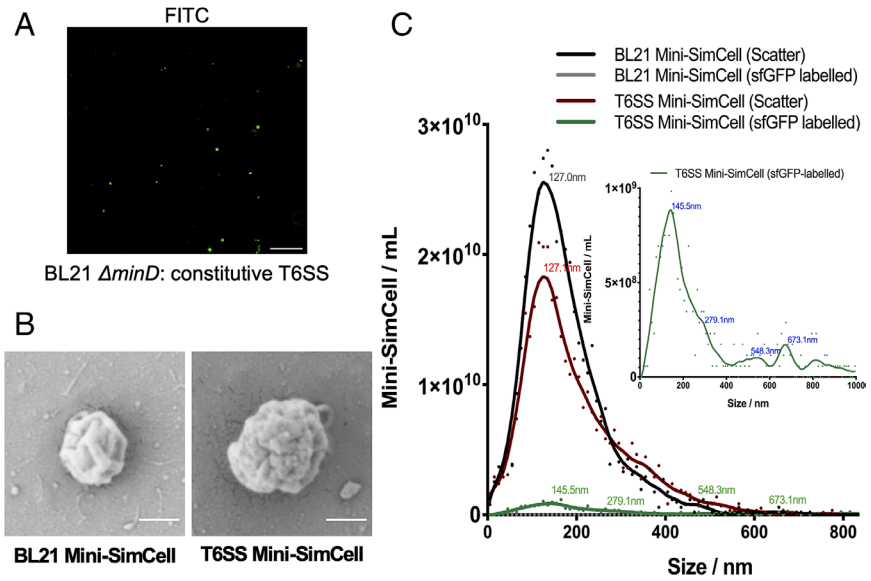

Fig. 3. Characterization of mini-SimCells with T6SS. (*A*) Fluorescence microscopic analysis confirms the assembly of T6SS in *E. coli* BL21(DE3)-derived mini-SimCells. (*B*) Scanning electron microscope images of mini-SimCells derived from BL21 parental cells with/without T6SS (T6SS/BL21 mini-SimCells). Magnification, 50,000×. (Scale bar, 200 nm.) (*C*) Size distribution characterization of mini-SimCells derived from BL21 parental cells with/without T6SS (T6SS/BL21 mini-SimCells). Characterization of size distribution and concentration using the ZetaView.

inhibitory concentration curve, the half-maximal inhibitory concentration (IC_{50}) of MOI of Nb-T6SS mini-SimCells was determined to be approximately 518.5 (*SI Appendix*, Fig. S6*C*). The results demonstrate the efficient prey-killing capability of our reprogrammed therapeutic mini-SimCells.

Localized H_2O_2 Generation from Parental Cells and (Mini-) SimCells. In addition to the T6SS system, close contact between attacker and prey cells also allows local delivery of high concentrations of antimicrobial compounds around the targeted cells. To exploit this, we introduced a constitutively expressed salicylate hydroxylase (NahG) into our system (*SI Appendix*, Fig. S8*A*), which catalyzes the conversion of acetylsalicylic acid (aspirin) into catechol (70, 71) (Fig. 4*A*). Catechol has a broad-spectrum antimicrobial activity (67–69) by generating hydrogen peroxide (H_2O_2) through auto-oxidation processes (*SI Appendix*, Fig. S7 *A*–*C*), during which catechol polymerizes to form cross-linked polymers without external catalysts (80–83) (Fig. 4*A*). When 800 μM aspirin [a nontoxic dose for humans (84)] was added to the parental cell and SimCell cultures, the filtered supernatants from overnight NahG+ cultures exhibited a dark-brown color (*SI Appendix*, Fig. S8*B*), which is associated with the oxidation products of catechol. The collected supernatants showed a significant inhibitory effect on bacterial cell growth (*SI Appendix*, Fig. S8 *B* and *C*). These results indicate the generation, permeability, and extracellular antimicrobial activity of SimCell-produced catechol and associated production of H_2O_2.

We then investigated coexpression of nanobody and NahG (Nb+NahG) in parental cells, SimCells, and mini-SimCells to eliminate targeted prey cells. The Nb+NahG parental cells, SimCells, and mini-SimCells were added to the prey cells at MOI of 10, 100, and 1,000, along with 800 μM aspirin. As shown in Fig. 4*B*, significant inhibition was apparent in 6 h and pronounced across all experimental groups by 24 h. Particularly after 48 h, Nb+NahG mini-SimCells eliminated over 99.9% of the prey cells in the presence of a single aspirin dose. These results demonstrate that the NahG reprogrammed SimCells provide a rapid and durable, aspirin-dependent antimicrobial effect.

Notably, NADH is required for NahG catalysis (71, 85). Prior studies suggest that mini-SimCells possess a higher NADH/NAD+ ratio (86, 87), likely due to the reduced electron transport chain activity resulting from the deletion of the *minD* gene and subsequent alterations in the activity of inner membrane enzymes (88, 89). Along with safety and a higher specific surface area (SSA)

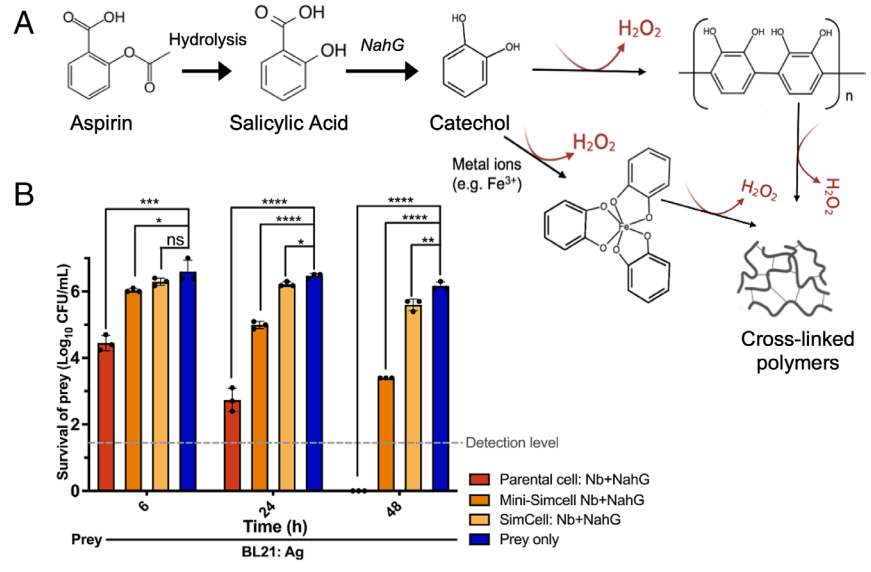

Fig. 4. Reprogrammed parental cells and (mini-) SimCells enables localized generation of antimicrobial compound—catechol. (*A*) Schematic depicting the hydrolysis of aspirin to salicylic acid, followed by the generation of catechol catalyzed by the NahG enzyme. The auto-oxidation of catechol and cross-linking results in the release of H_2O_2. (*B*) Inhibitory efficiency of localized catechol-producing parental cells/SimCells/Mini-SimCells. Attacker: prey n/n ratio = Parental cells/SimCells/Mini-SimCells 10/100:1,000:1. n = 3 replicates, Error bars, ±1 SD, **P* < 0.1, ***P* < 0.01, ****P* < 0.001, *****P* < 0.0001 according to a 2-tailed paired *t* test.

that enhances catechol penetration, mini-SimCells system is believed to be a promising platform and hence selected for further experiments.

Dual-Mechanism Killing Effect in Mini-SimCells. Building upon these results, we evaluated an integrated mini-SimCell strategy that combines nanobody-mediated binding, T6SS activity, and the localized release of an antimicrobial compound. To divide cellular burden and optimize the functionality of two different antimicrobial mechanisms (T6SS facilitated nano-needle and NahG mediated H_2O_2 local release), we employed a consortium of Nb+ mini-SimCells comprising two specialized subgroups: Attacker1 (mini-SimCell Nb-T6SS) and Attacker2 (mini-SimCell Nb-NahG). Nonengineered mini-SimCells (mini-SimCell Null) were used as negative controls. Antigen-positive prey cells were mixed and cocultured with various combinations of engineered and control mini-SimCells in the minimal medium. After 6 h, 800 μM aspirin was added. The T6SS-mediated attack was triggered immediately upon cell–cell contact, whereas H_2O_2-based killing began after catechol production from aspirin. Delaying catechol and subsequent H_2O_2 production potentially prevented these toxic metabolites from inhibiting T6SS activity. Prey cell viability was quantified at 6, 24, and 48 h without further additions of attacker cells or aspirin.

At an overall MOI of 250:250:1 (Attacker 1:Attacker 2:prey), each engineered mini-SimCell subgroup independently reduced prey viability at different time scales, confirming the efficacy of both antimicrobial modes. When combined, the dual-mechanism consortium achieved a significant killing effect at 6 h, as well as the greatest effect, eliminating approximately 90% of prey cells after 48 h, demonstrating an improved antimicrobial effect with two mechanisms (Fig. 5*A*). We next tested a higher dose dual-mechanism mini-SimCells to treat the target bacteria. Two types of attacker mini-SimCells were mixed with targeted prey cells at MOI of 500:500:1 (Attacker 1:Attacker 2:prey) with the total mini-SimCells of 1×10^{10}, the maximum tolerated dose reported in human minicell trials (79). Within the first 6 h, the Attacker1 (mini-SimCell engineered with Nb-T6SS) rapidly eliminated over 51% of the target bacteria. Addition of 800 μM aspirin enabled Attacker2 (mini-SimCell engineered with Nb-NahG) to convert aspirin to catechol and generate local H_2O_2 by polymerizing catechol, increasing the killing efficiency to 94.4 ± 0.73% at 24 h and further reaching 99.3% ±0.29% at 48 h (Fig. 5*B*).

To further evaluate the specificity and robustness of the platform in a complex environment, we applied a multidose mini-SimCells to selectively target Ag^+ bacteria population within a mixed microbial community. In this experiment, two distinct types of prey populations: *E. coli* BL21 with or without surface-displayed EPEA antigen (Ag+/Ag–) were continuously cocultured in a well-mixed condition. To mimic periodic wash-out scenario, the cultures were diluted 1/50 with fresh medium every 24 h, allowed to recover for 8 h, and then challenged with 10^{12} ++ mini-SimCells (1:1 ratio of Nb-T6SS mini-SimCells: Nb-nahG mini-SimCells) or an equivalent number of the control, which is nonengineered – – mini-SimCells (mini-SimCell without introduced plasmid). After each dose, cocultures were incubated for an additional 16 h to allow mini-SimCell mediated killing to run completely. In the presence of 800 μM aspirin, four sequential doses of mini-SimCells, selective elimination of the Ag+ population was observed only in the ++ mini-SimCells treatment group (Fig. 5*C*). Progressive elimination of Ag+ cells occurred following each dual-mechanism mini-SimCell administration, ultimately achieving a 10^3-fold reduction relative to the initial prey cell levels (Fig. 5*C*). This selective elimination was not observed in the

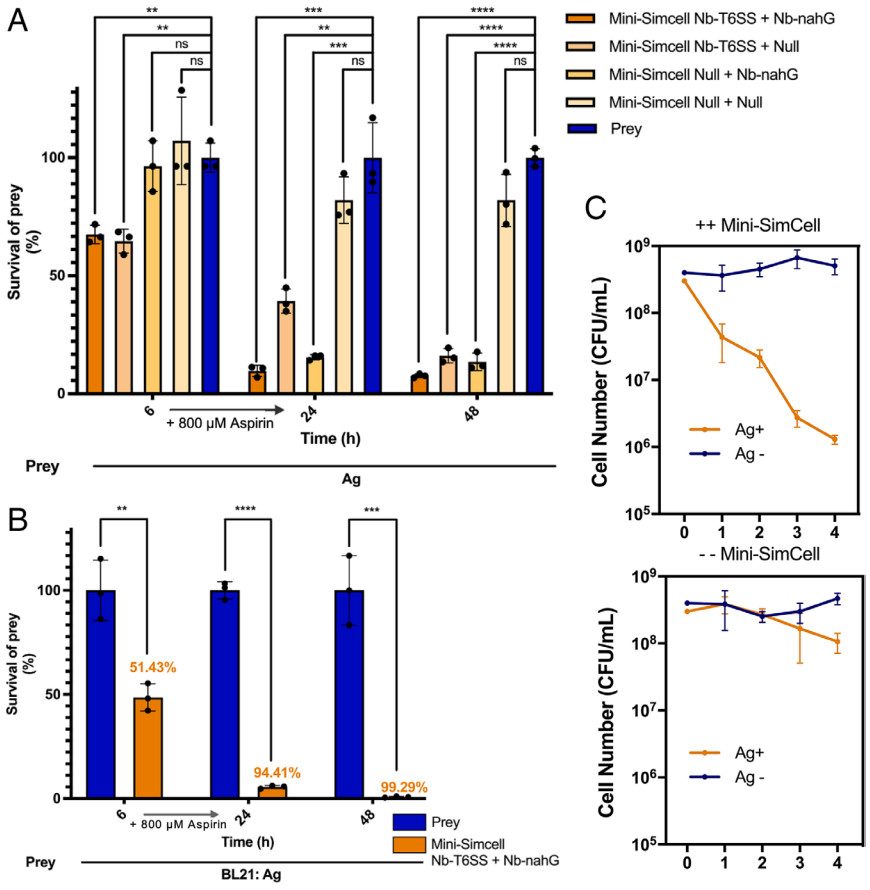

Fig. 5. Inhibitory efficiency of the consortium with dual-mechanism mini-SimCells in liquid condition. (*A*) Two different attackers (Attacker1: mini-SimCell Nb-T6SS; Attacker2: mini-SimCell Nb-nahG) were mixed with prey cells in n/n ratio of Attacker1: Attacker2: prey = 250:250:1, total Attaker cells were 5×10^9, within the maximum tolerated dose reported in the previous human trial. All cultures were incubated at 37 °C and sampled from 6 h, 24 h, 48 h. Aspirin of 800 μM was added after 6 h. (*B*) Dual-mechanism mini-SimCell inhibition efficiency in MTD (maximum tolerated dose) for humans. Two different attackers (Attacker1: mini-SimCell Nb-T6SS; Attacker2: mini-SimCell Nb-nahG) were mixed with prey cells in n/n ratio of Attacker1: Attacker2: prey = 500:500:1, total Attaker cells were 1×10^{10}, the maximum tolerated dose reported in the previous human trial. All cultures were incubated at 37 °C and sampled from 6 h, 24 h, 48 h. Aspirin of 800 μM was added after 6 h. (*C*) Specific depletion of targeted bacteria population in mixed communities using multidose dual-mechanism mini-SimCell consortium. Mixed prey cell populations with or without recognizable antigens (Ag+ or Ag–) were inoculated in n/n ratio of 1:1 for continuous coculture at 37 °C. 1/50 dilution with fresh medium was conducted every 24 h, followed by 8 h of recovery growth, then introduction of a dose of mini-SimCell consortium and 16 h of coincubation. For every dose of mini-SimCell consortium, two different attackers (Attacker1: mini-SimCell Nb-T6SS; Attacker2: mini-SimCell Nb-nahG) were mixed in n/n ratio of 1:1, total Attacker cells were 1×10^{12}. For – – Mini-SimCell group, 1×10^{12} of nonengineered mini-SimCell were used. All cultures were incubated at 37 °C and sampled every 24 h. Aspirin of 800 μM was added with fresh medium. For (*A* to *C*), n = 3 replicates, Error bars, ±1 SD, $^{**}P < 0.01$, $^{***}P < 0.001$, $^{****}P < 0.0001$ according to a 2-tailed paired *t* test. Survival rate was calculated as survival cells/ total prey cells. Killing efficiency was calculated as 1-survival rate.

control groups (– – mini-SimCell group), ruling out different growth rates between Ag+ and Ag– populations in the microbial community (Fig. 5*C*). Furthermore, the Ag– population remained stable throughout the treatment experiment, confirming the specificity of the target elimination (Fig. 5*C*).

To evaluate potential resistance could emerge against reprogrammed mini-SimCells, three colonies were isolated from surviving Ag+ populations after four consecutive doses of ++ mini-SimCell treatment, repopulated and rechallenged with fresh ++ mini-SimCells at MOI 1:1,000 for 24 h (*SI Appendix*, Fig. S9*A*). The resulting survivors still exhibited susceptibility comparable to the original Ag+ strains, indicating no detectable resistance development. Additionally, prey *E. coli* populations were serially passaged in M9 medium under ++ mini-SimCell or ciprofloxacin (a commonly used antibiotic) treatment. The ++ mini-SimCells (MOI of 1,000:1) and ciprofloxacin (0.00195 μg/mL) treatment were initiated a comparable intensity, each making over 99% killing efficiency in 48 h. In each round, all surviving colonies were pooled and used to inoculate the next passage rounds. Sensitivity of the population was quantitatively assessed after each passage. After four passages, prey cell populations exhibited no detectable reduction in susceptibility to ++ mini-SimCells, whereas parallel ciprofloxacin-treated populations showed two-to-three-order of magnitude increase of resistant colonies relative to the initial condition (*SI Appendix*, Fig. S9*B*). It suggests that resistance to the dual-mechanism reprogrammed mini-SimCell platform does not emerge readily under sustained selective pressure conditions which are sufficient to drive conventional antibiotic resistance evolution.

We also assessed potential cytotoxicity of reprogrammed mini-SimCells to mammalian cells. HEK293 cells were coincubated with reprogrammed (++) or nonengineered (– –) mini-SimCells at MOI of 1:10,000, 25,000, and 100,000 for 24 and 48 h, followed by live/dead fluorescence staining (*SI Appendix*, Fig. S10*A*) and viability quantification (*SI Appendix*, Fig. S10*B*). No off-target cytotoxicity was observed across all tested conditions and timepoints (*SI Appendix*, Fig. S10 *A* and *B*), indicating that mini-SimCells do not compromise mammalian cell viability even at high doses, supporting the safety profiles for in vivo therapeutic applications.

Collectively, these results demonstrate the potent and durable antimicrobial activity of dual-mechanism mini-SimCells. The combination of rapid T6SS-mediated killing with prolonged NahG-driven H_2O_2 production has effectively and selectively eradicated targeted cells in mixed communities while sparing nontarget populations.

Reprogrammed Mini-SimCells Effectively Targeted and Eliminated *E. coli* ST131, an AMR Pathogenic Strain. Building on the proof-of-concept platform demonstrating SimCell- and mini-SimCell-based targeted antimicrobial activities in mixed communities, we then evaluate the system against a clinically relevant multidrug-resistant pathogen. *E. coli* ST131 represents a globally dominant AMR strain responsible for a substantial proportion of urinary tract and bloodstream infections (90–93). It raises clinical concern particularly because of its resistance to fluoroquinolones and β-lactam antibiotics due to its extended-spectrum β-lactamases (ESBLs) (91, 94). The WHO has classified ESBL-producing *E. coli*, including ST131, as a high-to-critical priority AMR pathogen, underscoring the urgent need for novel therapeutic strategies targeting this AMR strain (95). Hence *E. coli* ST131 (NCTC 13441) strain was selected for the evaluation of the SimCell efficacy against AMR pathogens.

To achieve specific recognition of *E. coli* ST131, we engineered (mini-)SimCells to express nanobodies targeting outer membrane protein (OmpA). Specifically, we used Nb39, a nanobody exhibiting high binding affinity and specificity for the long OmpA isoform (OmpA-L) in *E. coli* isolates (96). Critically, the *E. coli* BL21(DE3) strain, which is used to generate mini-SimCells, expresses the short OmpA isoform (OmpA-S), which is not recognized by Nb39 (96). This isoform-specific binding provides a stringent negative control and prevents self-aggregation of attacker mini-SimCells. We engineered Nb39 fused with the N-terminal modular system for surface display in the parental strain of mini-SimCells. Stationary-phase cultures of *E. coli* ST131 and Nb39-displaying cells (BL21: Nb39-mRFP) were adjusted to the same OD_{600}, mixed at a 1:1 ratio, and allowed to settle overnight undisturbed. *E. coli* BL21(DE3) strains engineered with surface displayed synthetic antigen (BL21: Ag), EPEA, were used as the unrecognized control and mixed with Nb-39-displaying cells. *E. coli* ST131 and BL21: Ag cells were prestained with SYTO 9, while Nb39-displaying cells were genetically labeled with mRFP for fluorescence tracking. Fig. 6*A* shows parental cells (expressing mRFP) with Nb39 surface display bound to *E. coli* ST131 (SYTO9 staining). Significant cell–cell aggregates were observed under a fluorescence microscopy (Fig. 6 *A*, *Top*), while the control showed scattered cell distribution (Fig. 6 *A*, *Bottom*). Aggregation of these cells was mediated by the interactions of the OmpA-L antigen and Nb39 nanobody. Flow cytometry detected single events exhibiting both green and red fluorescence (G + R), designated as "doublets". Flow cytometry analysis demonstrated that 46.4% of the population exhibited doublet characteristics (Fig. 6*B*), while the control had 0.0% doublets (*SI Appendix*, Fig. S11*A*). It indicates the efficient targeting at *E. coli* ST131 via Nb39-mediated antigen recognition. These results confirm that surface-displayed Nb39 enables specific and robust binding to *E. coli* ST131 through native antigen (OmpA-L) recognition, preparing for the targeted mini-SimCells killing.

Subsequently, we demonstrate that reprogrammed mini-SimCells achieved efficient elimination of the multidrug-resistant pathogenic strain *E. coli* ST131 (Fig. 6*C*). Nb39-displaying mini-SimCells equipped with either T6SS (mini-SimCell: Nb39-T6SS) or nahG (mini-SimCell: Nb39-nahG) modules were evaluated for their antimicrobial efficacy. *E. coli* ST131 elimination assays were conducted at an overall MOI of 500:500:1 (Attacker 1: Attacker 2: Prey), with a total mini-SimCell number of 1×10^{10}. Nonengineered mini-SimCells (mini-SimCell Null) was used as control. Mini-SimCells equipped with nanobody-directed T6SS achieved >70% elimination of *E. coli* ST131 at 6 h (Fig. 6*C*). When 800 μM aspirin was supplemented, the converted catechol and locally generated H_2O_2 further enhanced antimicrobial activity. Hence, the dual-mechanism mini-SimCell consortium increased the elimination efficiency to 97.19% ±0.97% at 24 h and 97.58 ± 1.05% at 48 h (Fig. 6*C*). In contrast, *E. coli* ST131 exhibited persistent resistance to broad-spectrum β-lactam antibiotics, with no growth inhibition observed for benzylpenicillin (PenG) and cefotaxime even at 100 μg/mL (*SI Appendix*, Fig. S11 *B* and *C*). These results demonstrate that the nanobody-targeted, dual-mechanism mini-SimCell platform can overcome conventional antibiotic resistance mechanisms to achieve potent, specific elimination of clinically relevant multidrug-resistant pathogens.

Discussion

In this study, we introduce a SimCell and mini-SimCell platform with antimicrobial properties. Through nanobody–antigen binding, the reprogrammed SimCells and mini-SimCells are designed to selectively eliminate target cells via T6SS-mediated killing within 4 to 6 h and local conversion of aspirin to catechol, which then continuously generates high-concentration of H_2O_2 over several days. This antimicrobial strategy provides both immediate and sustained antimicrobial effects, offering the potential for

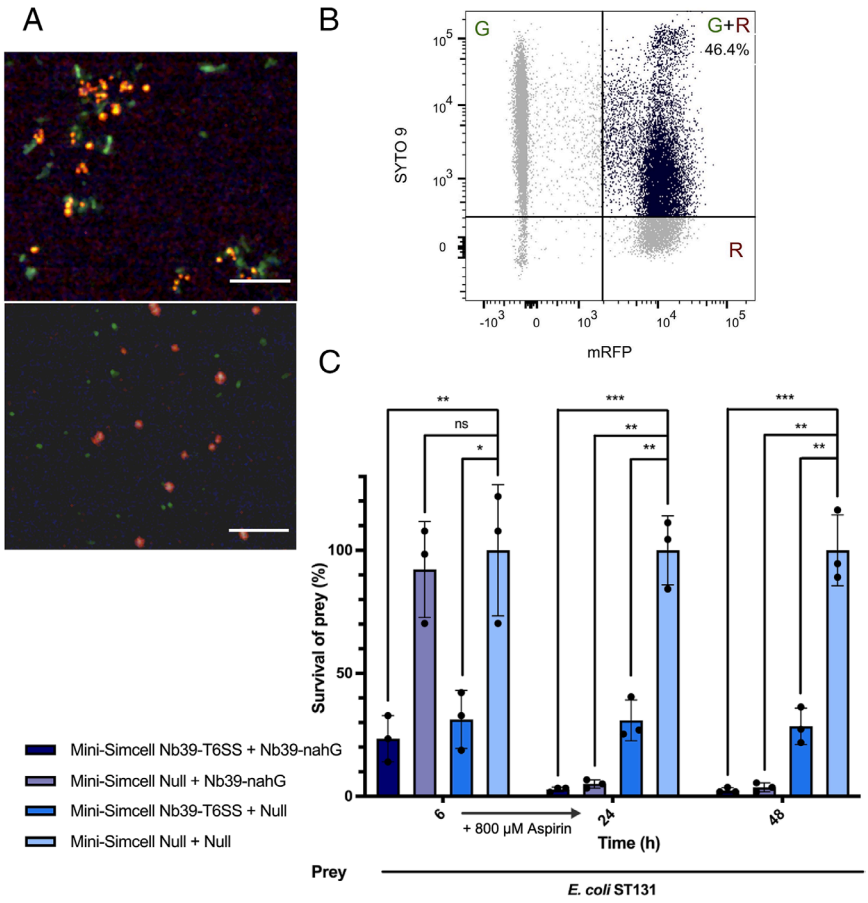

Fig. 6. Reprogrammed mini-SimCells to kill a resistant pathogenic *E. coli* strain (*E. coli* ST131) by targeting a native antigen (OmpA-L). (*A*) Binding of *E. coli* ST131 and BL21: Nb39_mRFP cells in a 1:1 ratio leads to significant aggregation observed under a fluorescence microscope. BL21: Ag cells were mixed with BL21: Nb39_mRFP cells as unbinding negative control. Red: BL21: Nb39_mRFP cells. Green: SYTO 9 stained *E. coli* ST131 cells (*Top*), SYTO 9 stained BL21: Ag cells (*Bottom*). (Scale bar, 10 μm.) (*B*) Quantification of Nb39-mediated *E. coli* ST131 binding using a double-color flow cytometry assay. Events of doublets formation (G + R) refers to the captured *E. coli* ST131 cells by cells displaying Nb39 nanobody. *E. coli* ST131: BL21: Nb39_mRFP cell = 1:1. (*C*) Inhibitory efficiency of the consortium with dual-mechanism mini-SimCells against *E. coli* ST131. Two different attackers (Attacker1: mini-SimCell Nb39-T6SS; Attaker2: mini-SimCell Nb39-nahG) were mixed with prey cells in n/n ratio of Attacker1: Attacker2: prey = 500:500:1, total Attaker cells were 1×10^{10}, align with the maximum tolerated dose reported in the previous human trial. All cultures were incubated at 37 °C and sampled from 6 h, 24 h, 48 h. Aspirin of 800 μM was added after 6 h. N = 3 replicates, Error bars, ±1 SD, $^{*}P < 0.1$, $^{**}P < 0.01$, $^{***}P < 0.001$ according to a 2-tailed paired *t* test. Survival rate was calculated as survival cells/ total prey cells.

controlling acute bacterial infection and preventing reoccurrence. For proof-of-concept, our results demonstrate that the mini-SimCell consortium can eliminate 94.4% of target prey cells in 24 h, and 99.3% in 48 h with a single dose of mini-SimCells at MOI of 1,000:1. Our results also demonstrate the selective pathogen depletion up to 10^3-fold within the mixed microbial communities using multidose mini-SimCell administration. This observation further validates the specific antimicrobial efficacy of the platform. To demonstrate the anti-AMR capacity and clinical application potential of our reprogrammed (mini-)SimCell-based therapeutic platform, we adapted the system to target the clinically relevant, multidrug-resistant pathogenic strain *E. coli* ST131. Equipped with a native OmpA recognizing nanobody (Nb39), our reprogrammed mini-SimCells achieved 97.19% target pathogen elimination within 24 h, overcoming conventional antibiotic resistance mechanisms. This success against a high-to-critical priority AMR pathogen demonstrates the translational potential of our platform for addressing urgent clinical challenges posed by multidrug-resistant infections. The combination of antibacterial efficacy and selectivity represents a significant advancement over broad-spectrum antimicrobial approaches, positioning this platform as a promising next-generation therapeutic strategy for combating antimicrobial resistance.

We vision this platform as an approach for developing clinically safe, custom-designable biotherapeutic products against multidrug-resistant pathogens. The key attributes and advantages of this platform include the following aspects: 1) Biosafety. SimCells and mini-SimCells met the criteria of NIH-recommended escape frequency threshold—one live cell from 10^8 SimCells (77). Preliminary in vitro coculture experiments demonstrate neglectable cytotoxicity of reprogrammed mini-SimCells to HEK293 mammalian cells even at high doses. Minicells derived from *Salmonella typhimurium,* which are similar to *E. coli* derived mini-SimCells, have been granted US FDA approval for human trial (https://engeneic.com/), and proven safe without adverse effect in human phase I clinical trial (97). To further enhance biosafety, our platform will be extended to use SimCells and mini-SimCells derived from LPS-free *E. coli* BL21(DE3) chassis (ClearColi) (98). 2) Antimicrobial specificity and efficacy. SimCell and mini-SimCell chassis are highly controllable while maintaining robust bioactivity against target bacteria. The precise targeting helps to minimize unintended effects on nontargeted microbes, enhancing the therapeutic efficacy. Further validation study in phylogenetically complex polymicrobial communities representing the native microbiomes will be critical for future clinical translation. 3) Modularity and customizability. This modular platform features a versatile architecture that allows for easy redesign in a "plug-and-play" manner. Surface-displayed nanobodies can be systematically reconfigured to target a specific new pathogen, enhancing the adaptability of the platform. Additionally, T6SS effectors can be engineered and seamlessly integrated into the existing modules. The enzyme-catalysis mechanism for converting pro-drugs to antimicrobial compounds, such as the aspirin-catechol system, can also be redesigned to fit specific therapeutic needs. 4) Scalability. SimCells and mini-SimCells can be easily produced and purified from engineered parent cells, making them suitable for large-scale industrial manufacturing. The streamlined production process, combined with high yield and cost-effective scalability, offers a manufacturing practical solution to address the urgent challenges posed by AMR.

The historic battle between humans and bacterial pathogens has intensified since the "Golden Age" of antibiotic discovery in the 1950s (8). Today, only a limited number of small molecules are currently undergoing clinical trials as potential antibiotic

candidates, with nearly half being new beta-lactamase inhibitors used with established beta-lactam antibiotics (99). Recent advances in AI and machine learning (ML) have accelerated antibiotic discovery and design. A landmark study employed a deep neural network to identify a novel broad-spectrum antibiotic, halicin (22), followed by works utilizing machine learning models to discover new antibiotics against drug-resistant *Acinetobacter baumannii* (19, 20). A recent work for the first time de novo designed structurally novel antibiotics for drug-resistant gonorrhea and MRSA via a generative deep learning approach (23). Despite these advances, the "black box" nature of some AI models can obscure the rationale behind predictions and limit the exploration of chemical spaces. Hence, researchers are now actively working on interpretable AI models (21). Additionally, validation of these in silico predictions and data collection for model training still requires extensive experimental tests.

Traditional chemical-based antibiotics face an evolutionary paradox: while effectively eliminating susceptible bacteria, they also promote the survival and spread of resistant variants, inadvertently advancing AMR with each treated infection (100). In response, alternative antimicrobials have been developed, including antimicrobial peptides, bacteriophage, and monoclonal antibodies. Each approach faces its challenges, such as biosafety, stability, and the potential risk of rapid resistance development (*SI Appendix*, Table S1). Several studies have reported the antimicrobial effects of bacteria engineered to neutralize virulence (101, 102) or eradicate pathogens. To selectively inhibit the target bacteria, toxic cargos were delivered by conditional lysis-based release (103, 104) or cytoplasm-translocation via conjugation (105–107). Nonetheless, balancing high efficacy with the management of side effects (e.g. endotoxin release during lysis) remains a challenge for these approaches. In contrast, the highly controllable and safe SimCells and mini-SimCells are reprogrammed to selectively target pathogens through surface-displayed nanobodies and efficiently eliminate the target cells, using contact-dependent antimicrobial strategies.

This study established a modular antimicrobial platform as proof of concept, and further successfully demonstrates its adaptability using a native-antigen-targeting nanobody against a multidrug-resistant pathogen from a clinical isolate. In real world clinical practice, the surface antigens of AMR pathogens could change due to mutations and environmental factors, potentially affecting epitope accessibility. The modularized design of mini-SimCell platform can be rapidly adapted to equip new nanobodies in response to the changes of surface antigens in AMR pathogens. We expect to further expand nanobody reservoirs targeting antigens from various multidrug-resistant pathogens and resembling diverse clinical scenarios. The current landscape of nanobody discovery relies on immunity-based approaches (108), which restricts diversity and availability. Emerging strategies, such as the combination of bioinformatics-driven antigen mining and high-throughput library (109, 110), AI enabled de novo protein design (111, 112) and deep learning models (113), offer promising approaches to overcome the limitations and accelerate the expansion of the nanobody repertoire for next generation of precise antimicrobials. Antigen mutations could possibly enable the prey cell to escape from being recognized and targeted. This antigen escape pathway could be mitigated through development of multi-nanobody cocktails targeting multiple independent surface antigens simultaneously.

T6SS represents a worth-noting strategy in this study. Building on previous research that uses native T6SS as controllable weapons against target pathogens (114, 115), our work advances the field by heterologously expressing and assembling functional T6SS in SimCell and mini-SimCell chassis, enhancing T6SS-based biotherapeutic applications. The natural diversity of T6SS's effectors and targets provides a foundation for expanding the functionality of engineered T6SS in this SimCell platform to antimicrobial-resistant (AMR) Gram-positive bacteria and fungi (116). Engineered T6SS could also deliver various protein payloads, such as Cas9 (117) and Cre recombinase (118), directly to the cytoplasm of target pathogens. SimCell and mini-SimCell chassis also minimize environment disruption in situ, with the versatility of T6SS opening possibilities for a wide range of biotherapeutic interventions (117) and ecological modification of microbial communities (119).

Based on current experimental results, no detectable resistance to reprogrammed mini-SimCell treatment was observed in target cell populations following four serial passages under sustained selective pressure. While it is uncertain how well these in vitro experimental conditions predict resistance emergence in clinical infection contexts and long-term evolution studies represent important priorities for clinical translation, the dual-mechanism T6SS "nano-needle" toxin delivery (120) and H_2O_2 mediated oxidative stress (121) are evolutionarily conserved antibacterial strategies. Multiple and functionally distinct T6SS toxins can effectively constrain resistance evolution in target bacteria (122). H_2O_2-mediated killing recapitulates the oxidative burst strategy central to human innate immune defense against bacteria (121), which remained effective throughout host-pathogen coevolution, suggesting fundamental evolutionary constraints on complete ROS resistance. To further minimize the likelihood risk of resistance development, the modularized "plug-and-play" antimicrobial platform can be readily expanded by engineering novel T6SS deliverable effectors and introducing alternative enzymes for localized conversion of pro-drugs into active antibacterial agents.

In conclusion, the reprogrammed antimicrobial SimCell and mini-SimCell platform described in this study offers an approach for tackling global bacterial AMR challenges. This work exemplifies the potential of synthetic biology to revolutionize biotherapeutic applications, demonstrating an innovative and effective approach to combat persistent and emerging AMR threats.

Materials and Methods

Bacterial Strains and Growth Conditions. All strains used in this study are listed in *SI Appendix*, Table S2. *E. coli* DH5α and DH10B were used for cloning and plasmid maintenance. *E. coli* BL21(DE3) was used for the function test and SimCell generation. *E. coli* BL21(DE3) ΔminD was used for mini-SimCell generation. Heat shock and electroporation methods were used for chemical transformation for both strains. Above cells were cultured in Luria−Bertani (LB) media or M9 minimal media with specific nutrient supplements (0.4% glucose, 0.2% casamino acids, 1x trace elements) at 37 °C, 180 rpm. *E. coli* ST131 (NCTC 13441) cells were cultured in M9 minimal media with 0.4% glucose and 1 mM EDTA at 37 °C, 180 rpm. Corresponding antibiotics were used for selection: 25 μg/mL chloramphenicol, 50 μg/mL kanamycin, 50 μg/mL carbenicillin, 100 μg/mL streptomycin, or 25 μg/mL cefotaxime. Corresponding inducers were used for induction: 100 ng/mL anhydrotetracycline (ATc), 0.2% arabinose (Ara), or 1 μM crystal violet. Strain stocks were stored in 20% glycerol at -80 °C for long-term storage. Agar plates were kept at 4 °C for short-term storage.

E. coli BL21(DE3) with pDSG287_sfGFP to express EPEA (*SI Appendix*, Table S2 and Dataset S1), and wild type pathogen *E. coli* ST131 were used as target bacteria. SimCells carrying pNb_NahG and pT6S_Tet (*SI Appendix*, Table S2 and Dataset S3) were used as therapeutic agents against *E. coli* BL21(DE3) with pDSG287_sfGFP (*SI Appendix*, Table S2 and Dataset S1). SimCells carrying pNb39_NahG and pTet_Nb39 (*SI Appendix*, Table S2 and Datasets S4 and S5) were used as therapeutic agents against *E. coli* ST131.

Plasmid Construction. All plasmids and primers used in this study are listed in *SI Appendix*, Table S2 and Tabl2 S3 separately. Plasmids were obtained from lab storage, purchased from Addgene (pDSG287, pDSG289, pDSG291) or as gifts from collaborators. Q5 high-fidelity DNA polymerase (New England Biolabs) was used for DNA fragment amplification. NEBuilder HiFi DNA Assembly (New England

Biolabs) was used for plasmid construction. DreamTaq Green PCR Master Mix (Thermo Fisher Scientific) was used for colony PCR. DNA stocks were stored at −20 °C.

Macroscopic and Microscopic Aggregation Assays. Cultures were grown at 37 °C, 180 rpm in 50 mL LB with corresponding antibiotics in a 200 mL flask for 24 h to ensure stationary phase. All cultures were centrifuged at 3,500 rpm for 20 min, resuspended with 1xPBS solution, then adjusted to an initial OD_{600} of 0.8. Cultures were mixed in a 1:1 v:v ratio (total volume 3 mL) in 5 mL clear polypropylene tubes. For macroscopic aggregation, 100 μL of sample was collected from the top 25% supernatant for each measurement. OD_{600} measurements were read by Synergy 2 microplate reader (BioTek). For microscopic aggregation, 100 μL of the sample was collected from the bottom of the overnight settled mixture and then diluted to an appropriate concentration for fluorescence microscopy using Nikon Ti Eclipse. Fiji was used for image analysis.

Bacterial Killing Assay. For parental cells, overnight cultures of attacker and prey cells were transferred into fresh LB medium with corresponding antibiotics at a ratio of 1:100 and grown to an $OD_{600} = 1$, the inducer was added when OD_{600} reached 0.6 if needed. Cells were harvested by centrifugation at 1,500 g for 10 min, and the pellets were resuspended in fresh LB or M9 minimal media. For SimCells and mini-SimCells, cell pellets were washed twice with fresh LB or M9 minimal media to fully remove the crystal violet or antibiotics. Cell suspensions were normalized to an initial OD_{600}. Mixtures of attacker and prey cells were then established at intended v:v or n:n ratios, cell number is calculated as (123, 124):

$$N_{\text{Parental cells/SimCells}} = A_{600} \times 8.0 \times 10^8/\text{mL},$$

$$N_{\text{mini\_SimCells}} = A_{600} \times 5.0 \times 10^{10}/\text{mL}.$$

For solid (contact-promoting) condition, triplicates of 5 μL of each mixture were spotted on LB/M9 agar plates (inducer was added if needed) and incubated at 37 °C for 3 h. Cells were then harvested by excising individual spots from the agar plates into LB medium. For liquid (well-mixed) conditions, mixtures of attacker and prey cells were established then incubated at 37 °C, 180 rpm for 2, 4, 6, 8, 24, 48 h. Suspensions were serially diluted and plated on selective media (selection for prey cells) for quantification of CFUs, then assessed the survival of prey cells. Survival rate was calculated as

$$\text{Survival rate} = \frac{\text{Survival cell}}{\text{total prey cell}} \times 100\,\%.$$

Killing efficiency was calculated as

$$\text{Killing (or elimination) efficiency} = 1 - \text{survival rate}$$

SimCell Purification and Characterization. For T6SS-assembled SimCells, overnight cultures were transferred into fresh LB medium with corresponding antibiotics at a ratio of 1:100 and grown at 37 °C, 180 rpm to an $OD_{600} = 1$, inducer was added when OD_{600} reached 0.6 if needed. For NahG-expressing SimCells, overnight cultures were directly used. Cells were collected by 1,500×*g* centrifuge for 10 min at room temperature, washed twice, and resuspended with M9 + 0.2% casamino acids media, inducer was added if needed. Crystal violet (1 μM) was added to induce plasmid pRH12x (*SI Appendix*, Table S2 and Dataset S2), converting *E. coli* into chromosome-free SimCell (48–50). Incubated overnight at 37 °C, 180 rpm. Then ceftriaxone (100 μg/mL), penicillin G (100 μg/ mL), and cefotaxime (100 μg/mL) were added to the culture and further incubated at 37 °C, 180 rpm for 4 h. 100 μL of cultures were plated for purity check and the rest were kept at 4 °C for further use. Cultures were washed twice with 1 × PBS to remove the crystal violet and antibiotics before being used for bacterial killing assay. Growth arrest assay: Overnight cultures were diluted in 1:1,000 ratio in 200 μL LB with corresponding antibiotics in a flat 96-well plate. The plate was sealed with a Breathe-Easy sealing membrane and incubated with Synergy 2 microplate reader (BioTek) at 37 °C, 1,000 rpm. OD_{600} was measured every 15 min since incubation. After 2-3 h, OD_{600} reached ~0.3, 0.2 μL of crystal violet to induce the SimCell conversion. OD_{600} were continuously measured for over 35 h. Plating assay: The culture (5 μL) from each group was extracted and dot-plated in LB agar without antibiotics. Plates were incubated for 24 h at 37 °C then images were collected to record the colony growth conditions.

Mini-SimCell Production and Purification. For T6SS-assembled mini-SimCells, overnight cultures were 1:100 inoculated into 100 mL fresh LB medium with corresponding antibiotics and grown at 37 °C, 180 rpm to an $OD_{600} = 1$, inducer was added when OD_{600} reached 0.6 if needed. For NahG-expressing SimCells, 100 mL of overnight cultures were directly used. The culture was centrifuged at 2,000×*g* for 10 min at 4 °C to remove the normal-size cells, the supernatant was retained for further centrifugation at 12,000 g for 15 min at 4 °C. The pellet was resuspended in 1 mL of fresh LB and pooled together. Ceftriaxone (100 μg/mL), penicillin G (100 μg/mL), and cefotaxime (100 μg/mL) were added to the culture and incubated at 37 °C, 180 rpm overnight. The culture was first centrifuged at 500×*g* for 10 min at 4 °C to remove cell debris. Then the supernatant was retained and further centrifuged at 12,000×*g* for 15 min at 4 °C to collect the mini-SimCells. The final pellet was resuspended in 1 mL of 1 × PBS solution and stored at 4 °C until further use. Cultures were washed twice with 1 × PBS to remove the antibiotics before being used for bacterial killing assay. 5 μL of each sample was used for plating assay to verify the purity.

Multidose Dual-Mechanism Mini-SimCell Consortium Killing Assay. *E. coli* with and without surface-displayed EPEA epitope were designated as Ag+ and Ag− strains respectively. Both strains were grown overnight in LB medium at 37 °C with shaking at 180 rpm, then normalized to an $OD_{600} = 1.25$. Equal volume (20 μL) of each culture was coinoculated into 1 mL of fresh LB in 1.5 mL Eppendorf tubes for 24 h to establish a steady status of the mixed population. Following incubation, 20 μL of each coculture was collected for serial dilution and plated on selective plates for prey cells and counted colony-forming units (CFUs), defining this as Day 0. Aspirin was then added into LB medium with a final concentration of 800 μM. Fresh mini-SimCells were prepared daily for every treatment dose. The engineered dual-mechanism ++ mini-SimCells consisted of Attacker1: mini-SimCell Nb-T6SS and Attacker2: mini-SimCell Nb-NahG at an n:n ratio of 1:1. The nonengineered − − mini-SimCells were served as negative control. For each dose, 100 μL 10^{12} ++/− − mini-SimCells were well mixed and then added into the coculture. The first dose of ++/− − mini-SimCells was added after initial 24-hr incubation, followed by an additional 16 h incubation at 37 °C, 180 rpm. Afterward, 20 μL of the cocultures were collected for plating and CFU counting (Day 1). The cocultures were then diluted 1:50 into fresh LB medium containing 800 μM aspirin, and incubated at 37 °C, 180 rpm for 8 h. This process was repeated for the 2nd, 3rd, 4th doses of mini-SimCells (Day 2, 3, and 4).

Cytotoxicity Assessment of Mini-SimCells to HEK293 Mammalian Cells. 5,000 cells/well HEK293 cells were seeded in a μ-Slide 8-Well high Glass Bottom (ibidi) with 0.2 mL fresh media (DMEM+10% FBS). Purified ++ and - - mini-SimCells were resuspended in DMEM+10% FBS medium and added in with MOI 10,000/25,000/100,000:1, mini-SimCells to HEK293 cell ratio. Min-SimCells and HEK293 cells were then coincubated at 37 °C with 5% CO2 for 24, 48 h. As positive control, HEK293 cells were treated with 70% ethanol for 10 min before staining. Hoechst 33342 (Invitrogen) and TOTO-3 Iodide (Invitrogen) were added into each well in a final concentration of 1.6 μM and 100 nM for total/death cell staining. Cells were incubated at 37 °C for 15 min then used for imaging using Nikon microscope. Each well was viewed under brightfield or fluorescent illuminance using a 40× objective (excitation/emission 488/510 nm for sfGFP; excitation/emission 350/461 nm for Hoechst 33342; excitation/emission 642/660 nm for TOTO-3 Iodide). ImageJ was used for image process and analysis.

Double-Color Flow Cytometry Assay for Binding Population Quantification. Overnight *E. coli* ST131 cultures were 1:100 inoculated in 5 mL M9 minimal media with 0.4% glucose and 1 mM EDTA, then grew at 37 °C, 180 rpm for 48 h. BL21:Ag and BL21: Nb39-mRFP strains were 1:100 inoculated at 37 °C, 180 rpm in 5 mL LB medium and grew overnight. All cultures were centrifuged at 1.500×*g* for 10 min, washed twice, and resuspended with 1 mL 1 × PBS solution. *E. coli* ST131 and BL21:Ag cultures were stained with 1 μM of SYTO 9 dye at room temperature for 2 h in the dark. Then all cultures washed twice with 1xPBS solution and resuspended with 1 × PBS solution, OD_{600} normalized to 1.0. *E. coli* ST131/ BL21:Ag and BL21: Nb39-mRFP cultures were mixed in v:v/1:1 ratio in total volume of 1.5 mL. Mixed cultures were settled still in the dark overnight. Each culture was 1:100 diluted with 1 × PBS solution and used for FACS analysis. BD Aria Fusion was used for flow cytometry analysis.

Data, Materials, and Software Availability. All study data are included in the article and/or supporting information. Annotated key plasmid sequence data are included in Datasets S1–S5.

ACKNOWLEDGMENTS. W.E.H. thanks EPSRC (EP/M002403/1 and EP/Y014073/1) for financial support. Y.D. gratefully acknowledges support from Oxford Interdisciplinary Bioscience DTP, funded by BBSRC (BB/T008784/1). K.R.F. is funded by Wellcome Trust Investigator award 209397/Z/17/Z and European Research Council Grant 787932. We thank Harris Saeed from the Engineering Department, University of Oxford, for helping with the SEM. Sample process and image for SEM were conducted at the Sir William Dunn School of Pathology, University of Oxford. We would like to acknowledge Dr. Naveed Akbar from the Radcliffe Department of Medicine, University of Oxford, for providing ZetaView equipment and technical expertise, Dr. Nina Wei from the Engineering Department, University of Oxford, for helping with mammalian cell culture and cytotoxicity experiments, and Vasiliki Tsioligka from the Flow Cytometry Facility, Sir William Dunn School of Pathology, University of Oxford, for providing flow cytometry technical expertise. We also thank all members of the Huang lab for the discussions and support.

Author affiliations: [a]Department of Engineering Science, University of Oxford, Oxford OX1 3PJ, United Kingdom; [b]Oxford Suzhou Centre for Advanced Research, University of Oxford, Jiangsu 215123, P.R. China; [c]Department of Immunology and Microbiology, School of Life Sciences, Southern University of Science and Technology, Shenzhen 518055, China; [d]Sir William Dunn School of Pathology, University of Oxford, Oxford OX1 3RE, United Kingdom; and [e]Department of Biological Sciences, University of Calgary, Calgary T2N 1N4, Canada

1. Antimicrobial resistance, https://www.who.int/health-topics/antimicrobial-resistance [Accessed 1 December 2024].
2. WHO, "WHO bacterial priority pathogens list, 2024: Bacterial pathogens of public health importance to guide research, development and strategies to prevent and control antimicrobial resistance" in *Bacterial Pathogens of Public Health Importance to Guide Research, Development and Strategies to Prevent and Control Antimicrobial Resistance* (2024), vol. **72**.
3. M. Naghavi *et al.*, Global burden of bacterial antimicrobial resistance 1990–2021: A systematic analysis with forecasts to 2050. *Lancet* **404**, 1199–1226 (2024).
4. J. O'Neill, Tackling drug-resistant infections globally: final report and recommendations (2016). https://amr-review.org/sites/default/files/160518_Final%20paper_with%20cover.pdf. Accessed 15 October 2024.
5. C. J. Murray *et al.*, Global burden of bacterial antimicrobial resistance in 2019: A systematic analysis. *Lancet* **399**, 629–655 (2022).
6. Global AMR R&D Hub and WHO, Incentivising the development of new antibacterial treatments 2024: Progress report by the global AMR R&D Hub and WHO (2024). https://globalamrhub.org/publications/incentivising-the-development-of-new-antibacterial-treatments-2024-progress-report-by-the-global-amr-rd-hub-and-who/. Accessed 20 November 2024.
7. M. Miethke *et al.*, Towards the sustainable discovery and development of new antibiotics. *Nature Rev. Chem.* **10**, 726–749 (2021).
8. L. L. Silver, Challenges of antibacterial discovery. *Clin. Microbiol. Rev.* **24**, 71–109 (2011).
9. C. Zampaloni *et al.*, A novel antibiotic class targeting the lipopolysaccharide transporter. *Nature* **625**, 566–571 (2024).
10. P. M. Wright, I. B. Seiple, A. G. Myers, The evolving role of chemical synthesis in antibacterial drug discovery. *Angew. Chem. Int. Ed.* **53**, 8840–8869 (2014).
11. B. Goel, N. Tripathi, N. Bhardwaj, I. Pal. Singh, S. K. Jain, Semisynthesis: An essential tool for antibiotics drug discovery. *ChemistrySelect* **9**, e202400554 (2024).
12. N. J. Ayon, High-throughput screening of natural product and synthetic molecule libraries for antibacterial drug discovery. *Metabolites* **13**, 625 (2023).
13. B. Blasco *et al.*, High-throughput screening of small-molecules libraries identified antibacterials against clinically relevant multidrug-resistant *A. baumannii* and *K. pneumoniae*. *EBioMedicine* **102**, 105073 (2024).
14. T. C. Scanlon, S. M. Dostal, K. E. Griswold, A high-throughput screen for antibiotic drug discovery. *Biotechnol. Bioeng.* **111**, 232–243 (2014).
15. G. König *et al.*, Rational prioritization strategy allows the design of macrolide derivatives that overcome antibiotic resistance. *Proc. Natl. Acad. Sci. U.S.A.* **118**, e2113632118 (2021).
16. T. F. Durand-Reville *et al.*, Rational design of a new antibiotic class for drug-resistant infections. *Nature* **597**, 698–702 (2021).
17. R. D. Miller *et al.*, Computational identification of a systemic antibiotic for gram-negative bacteria. *Nat. Microbiol.* **7**, 1661 (2022).
18. A. Talat, A. U. Khan, Artificial intelligence as a smart approach to develop antimicrobial drug molecules: A paradigm to combat drug-resistant infections. *Drug Discov. Today* **28**, 103491 (2023).
19. K. Swanson *et al.*, Generative AI for designing and validating easily synthesizable and structurally novel antibiotics. *Nature Mach. Intell.* **36**, 338–353 (2024).
20. G. Liu *et al.*, Deep learning-guided discovery of an antibiotic targeting Acinetobacter baumannii. *Nature Chem. Biol.* **19**, 1342–1350 (2023).
21. F. Wong *et al.*, Discovery of a structural class of antibiotics with explainable deep learning. *Nature* **626**, 177–185 (2023).
22. J. M. Stokes *et al.*, A deep learning approach to antibiotic discovery. *Cell* **180**, 688–702.e13 (2020).
23. A. Krishnan *et al.*, A generative deep learning approach to de novo antibiotic design. *Cell* **188**, 5962–5979.e22 (2025).
24. N. S. Devi *et al.*, Overview of antimicrobial resistance and mechanisms: The relative status of the past and current. *Microbe* **3**, 100083 (2024).
25. A. Bruttin, H. Brüssow, Human volunteers receiving *Escherichia coli* phage T4 orally: A safety test of phage therapy. *Antimicrob. Agents Chemother.* **49**, 2874–2878 (2005).
26. A. Wright, C. H. Hawkins, E. E. Änggård, D. R. Harper, A controlled clinical trial of a therapeutic bacteriophage preparation in chronic otitis due to antibiotic-resistant Pseudomonas aeruginosa; a preliminary report of efficacy. *Clin. Otolaryngol.* **34**, 349–357 (2009).
27. E. Criscuolo, S. Spadini, J. Lamanna, M. Ferro, R. Burioni, Bacteriophages and Their Immunological Applications against Infectious Threats. *J. Immunol. Res.* **2017**, 3780697 (2017).
28. A. DiGiandomenico, B. R. Sellman, Antibacterial monoclonal antibodies: The next generation? *Curr. Opin. Microbiol.* **27**, 78–85 (2015).
29. I. Lowy *et al.*, Treatment with Monoclonal antibodies against Clostridium difficile Toxins. *New Engl. J. Med.* **362**, 197–205 (2010).
30. L. M. Guachalla *et al.*, Multiple modes of action of a monoclonal antibody against multidrug-resistant *Escherichia coli* sequence type 131–H30. *Antimicrob. Agents Chemother.* **61**, e01428-17 (2017).
31. C. D. Fjell, J. A. Hiss, R. E. W. Hancock, G. Schneider, Designing antimicrobial peptides: form follows function. *Nat. Rev. Drug Discovery* **11**, 37–51 (2011).
32. C. D. Santos-Júnior *et al.*, Discovery of antimicrobial peptides in the global microbiome with machine learning. *Cell* **187**, 3761–3778.e16 (2024).
33. C. Bucataru, C. Ciobanasu, Antimicrobial peptides: Opportunities and challenges in overcoming resistance. *Microbiol. Res.* **286**, 127822 (2024).
34. F. Plisson, O. Ramírez-Sánchez, C. Martínez-Hernández, Machine learning-guided discovery and design of non-hemolytic peptides. *Sci. Rep.* **10**, 1–19 (2020).
35. F. L. Gordillo Altamirano, J. J. Barr, Phage therapy in the postantibiotic era. *Clin. Microbiol. Rev.* **32**, e00066-18 (2019).
36. U.S. Department of Health and Human Services Food and Drug Administration, Early clinical trials with live biotherapeutic products: Chemistry, manufacturing, and control information; Guidance for Industry (2016). https://www.fda.gov/regulatory-information/search-fda-guidance-documents/early-clinical-trials-live-biotherapeutic-products-chemistry-manufacturing-and-control-information. Accessed 16 April 2024.
37. D. T. Riglar, P. A. Silver, Engineering bacteria for diagnostic and therapeutic applications. *Nat. Rev. Microbiol.* **16**, 214–225 (2018).
38. A. Cubillos-Ruiz *et al.*, Engineering living therapeutics with synthetic biology. *Nat. Rev. Drug Discovery* **20**, 941–960 (2021).
39. M. Mimee, R. J. Citorik, T. K. Lu, Microbiome therapeutics–Advances and challenges. *Adv. Drug Deliv. Rev.* **105**, 44–54 (2016).
40. T. V. Plavec, A. Berlec, Engineering of lactic acid bacteria for delivery of therapeutic proteins and peptides. *Appl. Microbiol. Biotechnol.* **103**, 2053–2066 (2019).
41. J. P. Lynch, L. Goers, C. F. Lesser, Emerging strategies for engineering *Escherichia coli* Nissle 1917-based therapeutics. *Trends Pharmacol. Sci.* **43**, 772–786 (2022).
42. U. Sonnenborn, *Escherichia coli* strain Nissle 1917–from bench to bedside and back: History of a special *Escherichia coli* strain with probiotic properties. *FEMS Microbiol. Lett.* **363**, fnw212 (2016).
43. A. Wallecha, P. C. Maciag, S. Rivera, Y. Paterson, V. Shahabi, Construction and characterization of an attenuated Listeria monocytogenes strain for clinical use in cancer immunotherapy. *Clin. Vaccine Immunol.* **16**, 96–103 (2009).
44. R. P. Aganja, C. Sivasankar, A. Senevirathne, J. H. Lee, Salmonella as a promising curative tool against cancer. *Pharmaceutics* **14**, 2100 (2022).
45. M. Loeffler, G. Le'Negrate, M. Krajewska, J. C. Reed, Attenuated Salmonella engineered to produce human cytokine LIGHT inhibit tumor growth. *Proc. Natl. Acad. Sci. U.S.A.* **104**, 12879–12883 (2007).
46. C. T. Y. Chan, J. W. Lee, D. E. Cameron, C. J. Bashor, J. J. Collins, "Deadman" and "Passcode" microbial kill switches for bacterial containment. *Nat. Chem. Biol.* **12**, 82–86 (2015).
47. M. Zhao *et al.*, Tumor-targeting bacterial therapy with amino acid auxotrophs of GFP-expressing Salmonella typhimurium. *Proc. Natl. Acad. Sci. U.S.A.* **102**, 755–760 (2005).
48. C. Fan *et al.*, Chromosome-free bacterial cells are safe and programmable platforms for synthetic biology. *Proc. Natl. Acad. Sci. U.S.A.* **117**, 6752–6761 (2020).
49. B. Lim *et al.*, Reprogramming synthetic cells for targeted cancer therapy. *ACS Synth. Biol.* **11**, 1349–1360 (2022).
50. C. P. N. Rampley *et al.*, Development of SimCells as a novel chassis for functional biosensors. *Sci. Rep.* **7**, 1–10 (2017).
51. Y. Yin *et al.*, Engineering genome-free bacterial cells for effective SARS-COV-2 neutralisation. *Microb. Biotechnol.* **18**, e70109 (2025).
52. S. L. Liu, A. Hessel, K. E. Sanderson, Genomic mapping with I-Ceu I, an intron-encoded endonuclease specific for genes for ribosomal RNA, in Salmonella spp., Escherichia coli, and other bacteria. *Proc. Natl. Acad. Sci. U.S.A.* **90**, 6874 (1993).
53. H. I. Adler, W. D. Fisher, A. Cohen, A. A. Hardigree, Miniature escherichia coli Cells Deficient in DNA. *Proc. Natl. Acad. Sci.* **57**, 321–326 (1967).
54. J. A. MacDiarmid *et al.*, Bacterially derived 400 nm particles for encapsulation and cancer cell targeting of chemotherapeutics. *Cancer Cell* **11**, 431–445 (2007).
55. J. Lutkenhaus, Assembly dynamics of the bacterial minCDE system and spatial regulation of the z ring. *Annu. Rev. Biochem.* **76**, 539–562 (2007).
56. D. Thi Thanh Vinh, N. Tu Hoang Khue, Study on minicell generation of *Lactobacillus acidophilus* VTCC-B-871 for drug delivery article info abstract. *J. Appl. Pharm. Sci.* **3**, 33–036 (2013).
57. EnGeneIC granted FDA "Fast-Track" Designation for Novel Armed Nanocell Drug Conjugate (ANDC) pancreatic cancer therapeutic (2023). https://firstwordpharma.com/story/5808266. Accessed 27 December 2025.
58. J. A. MacDiarmid, H. Brahmbhatt, Minicells: Versatile vectors for targeted drug or si/shRNA cancer therapy. *Curr. Opin. Biotechnol.* **22**, 909–916 (2011).
59. S. M. Sagnella *et al.*, Cyto-immuno-therapy for cancer: A pathway elicited by tumor-targeted, cytotoxic drug-packaged bacterially derived nanocells. *Cancer Cell* **37**, 354–370.e7 (2020).
60. D. S. Glass, I. H. Riedel-Kruse, A synthetic bacterial cell-cell adhesion toolbox for programming multicellular morphologies and patterns. *Cell* **174**, 649–658.e16 (2018).
61. S. Pukatzki *et al.*, Identification of a conserved bacterial protein secretion system in *Vibrio cholerae* using the *Dictyostelium* host model system. *Proc. Natl. Acad. Sci. U.S.A.* **103**, 1528–1533 (2006).
62. J. D. Mougous *et al.*, A virulence locus of Pseudomonas aeruginosa encodes a protein secretion apparatus. *Science* **1979**, 1526–1530 (2006).

63. Y. Cui *et al.*, Heterologous assembly of the type VI secretion system empowers laboratory *Escherichia coli* with antimicrobial and cell penetration capabilities. *Appl. Environ. Microbiol.* **88**, e01305-22 (2022).
64. A. B. Russell *et al.*, Type VI secretion delivers bacteriolytic effectors to target cells. *Nature* **475**, 343 (2011).
65. S. J. Coulthurst, The Type VI secretion system – a widespread and versatile cell targeting system. *Res. Microbiol.* **164**, 640–654 (2013).
66. L. P. Allsopp, P. Bernal, Killing in the name of: T6SS structure and effector diversity. *Microbiology (United Kingdom)* **169**, 001367 (2023).
67. I. Kocaçalıskan, I. Talan, I. Terzi, Antimicrobial activity of catechol and pyrogallol as allelochemicals. *Z Naturforsch C J. Biosci.* **61**, 639–642 (2006).
68. N. Schweigert, A. J. B. Zehnder, R. I. L. Eggen, Chemical properties of catechols and their molecular modes of toxic action in cells, from microorganisms to mammals. *Environ. Microbiol.* **3**, 81–91 (2001).
69. S. Razaviamri, K. Wang, B. Liu, B. P. Lee, Catechol-based antimicrobial polymers. *Molecules* **26**, 559 (2021).
70. D. M. A. Costa *et al.*, Catalytic mechanism for the conversion of salicylate into catechol by the flavin-dependent monooxygenase salicylate hydroxylase. *Int. J. Biol. Macromol.* **129**, 588–600 (2019).
71. S. Yamamotoj, M. Katagiri, H. Maeno, O. Hayaishi, Salicylate hydroxylase, a monooxygenase* requiring flavin adenine dinucleotide I. Purification and general properties i. *J. Biol. Chem.* **240**, 3408–3413 (1965).
72. E. J. De Genst *et al.*, Structure and properties of a complex of α-synuclein and a single-domain camelid antibody. *J. Mol. Biol.* **402**, 326–343 (2010).
73. T. T. Pei *et al.*, Intramolecular chaperone-mediated secretion of an Rhs effector toxin by a type VI secretion system. *Nat. Commun.* **11**, 1–13 (2020).
74. X. Liang *et al.*, Characterization of lysozyme-like effector TseP reveals the dependence of type VI secretion system (T6SS) secretion on effectors in *Aeromonas dhakensis* strain SSU. *Appl. Environ. Microbiol.* **87**, e00435-21 (2021).
75. M. LeRoux *et al.*, Quantitative single-cell characterization of bacterial interactions reveals type VI secretion is a double-edged sword. *Proc. Natl. Acad. Sci. U.S.A.* **109**, 19804–19809 (2012).
76. T. Rollenske *et al.*, Parallelism of intestinal secretory IgA shapes functional microbial fitness. *Nature* **598**, 657–661 (2021).
77. Department of Health and Human Services National Institutes of Health, *NIH Guidelines for Research Involving Recombinant or Synthetic Nucleic Acid Molecules* (NIH Guidelines, 2024).
78. Y. G. Santin, T. Doan, L. Journet, E. Cascales, Cell width dictates type VI secretion tail length. *Current Biol.* **29**, 3707–3713.e3 (2019).
79. B. J. Solomon *et al.*, A first-time-in-human phase I clinical trial of bispecific antibody-targeted. Paclitaxel-packaged bacterial minicells. *PLoS One* **10**, e0144559 (2015).
80. J. Yang, M. A. Cohen Stuart, M. Kamperman, Jack of all trades: Versatile catechol crosslinking mechanisms. *Chem. Soc. Rev.* **43**, 8271–8298 (2014).
81. D. E. Fullenkamp, D. G. Barrett, D. R. Miller, J. W. Kurutz, P. B. Messersmith, pH-dependent cross-linking of catechols through oxidation via Fe3+ and potential implications for mussel adhesion. *RSC Adv.* **4**, 25127–25134 (2014).
82. H. Meng, Y. Li, M. Faust, S. Konst, B. P. Lee, Hydrogen peroxide generation and biocompatibility of hydrogel-bound mussel adhesive moiety. *Acta Biomater.* **17**, 160–169 (2015).
83. H. Meng *et al.*, Biomimetic recyclable microgels for on-demand generation of hydrogen peroxide and antipathogenic application. *Acta Biomater.* **83**, 109–118 (2019).
84. J. X. Chen *et al.*, Development of aspirininducible biosensors in *Escherichia coli* and SimCells. *Appl. Environ. Microbiol.* **85**, e02959-18 (2019).
85. M. Katagiri, S. Yamamoto, O. Hayaishi, Flavin adenine dinucleotide requirement for the enzymic hydroxylation and decarboxylation of salicylic acid. *J. Biolog. Chem.* **237**, PC2413–PC2414 (1962).
86. S. J. Kim, M. K. Oh, Minicell-forming *Escherichia coli* mutant with increased chemical production capacity and tolerance to toxic compounds. *Bioresour. Technol.* **371**, 128586 (2023).
87. S. J. Kim, W. Chang, M. K. Oh, Escherichia coli minicells with targeted enzymes as bioreactors for producing toxic compounds. *Metab. Eng.* **73**, 214–224 (2022).
88. H. L. Lee *et al.*, Quantitative proteomics analysis reveals the min system of Escherichia coli modulates reversible protein association with the inner membrane. *Mol. Cell. Proteomics* **15**, 1572–1583 (2016).
89. L. Wettmann, K. Kruse, The Min-protein oscillations in *Escherichia coli*: An example of self-organized cellular protein waves. *Philos. Trans. R. Soc. Lond. B Biol. Sci.* **373**, 20170111 (2018).
90. M. H. Nicolas-Chanoine, X. Bertrand, J. Y. Madec, Escherichia coli ST131, an intriguing clonal group. *Clin. Microbiol. Rev.* **27**, 543 (2014).
91. B. A. Rogers, H. E. Sidjabat, D. L. Paterson, Escherichia coli O25b-ST131: A pandemic, multiresistant, community-associated strain. *J. Antimicrob. Chemother.* **66**, 1–14 (2011).
92. M. H. Nicolas-Chanoine *et al.*, Intercontinental emergence of *Escherichia coli* clone O25:H4-ST131 producing CTX-M-15. *J. Antimicrob. Chemother.* **61**, 273–281 (2008).
93. A. Colpan *et al.*, Escherichia coli sequence type 131 (ST131) subclone H30 as an emergent multidrug-resistant pathogen among US Veterans. *Clinical Infectious Dis.* **57**, 1256–1265 (2013).
94. R. Banerjee, J. R. Johnson, A new clone sweeps clean: The enigmatic emergence of *Escherichia coli* sequence type 131. *Antimicrob. Agents Chemother.* **58**, 4997–5004 (2014).
95. World Health Organization, WHO Bacterial Priority Pathogens List, 2024- Bacterial pathogens of public health importance to guide research, development and strategies to prevent and control antimicrobial resistance. (World Health Organization, 2024), pp. 1–72.
96. M. Sorgenfrei *et al.*, Rapid detection and capture of clinical *Escherichia coli* strains mediated by OmpA-targeting nanobodies. *Commun. Biol.* **8**, 1–17 (2025).
97. B. J. Solomon *et al.*, A first-time-in-human phase I clinical trial of bispecific antibody-targeted. Paclitaxel-packaged bacterial minicells. *PLoS One* **10**, e0144559 (2015).
98. U. Mamat *et al.*, Endotoxin-free protein production–ClearColiTM technology. *Nature Methods* **10**, 916–916 (2013).
99. D. L. Paterson, Antibacterial agents active against Gram Negative Bacilli in phase I, II, or III clinical trials. *Expert Opin. Investig. Drugs* **33**, 371–387 (2024).
100. G. Cheng *et al.*, Antimicrobial drugs in fighting against antimicrobial resistance. *Front. Microbiol.* **7**, 470 (2016).
101. A. Focareta, J. C. Paton, R. Morona, J. Cook, A. W. Paton, A recombinant probiotic for treatment and prevention of cholera. *Gastroenterology* **130**, 1688–1695 (2006).
102. F. Duan, J. C. March, Engineered bacterial communication prevents *Vibrio cholerae* virulence in an infant mouse model. *Proc. Natl. Acad. Sci. U.S.A.* **107**, 11260–11264 (2010).
103. P. Jayaraman, M. B. Holowko, J. W. Yeoh, S. Lim, C. L. Poh, Repurposing a Two-Component System–Based Biosensor for the Killing of Vibrio cholerae. *ACS Synth. Biol.* **6**, 1403–1415 (2017).
104. I. Y. Hwang *et al.*, Engineered probiotic Escherichia coli can eliminate and prevent Pseudomonas aeruginosa gut infection in animal models. *Nature Commun.* **8**, 1–11 (2017).
105. T. A. Hamilton *et al.*, Efficient inter-species conjugative transfer of a CRISPR nuclease for targeted bacterial killing. *Nature Commun.* **10**, 1–9 (2019).
106. R. López-Igual, J. Bernal-Bayard, A. Rodríguez-Patón, J. M. Ghigo, D. Mazel, Engineered toxin–intein antimicrobials can selectively target and kill antibiotic-resistant bacteria in mixed populations. *Nature Biotechnol.* **37**, 755–760 (2019).
107. Y. G. Li, K. Kishida, N. Ogawa-Kishida, P. J. Christie, Ligand-displaying *Escherichia coli* cells and minicells for programmable delivery of toxic payloads via type IV secretion systems. *MBio* **14**, e02143-23 (2023).
108. S. Muyldermans, Nanobodies: Natural single-domain antibodies. *Annu. Rev. Biochem.* **82**, 775–797 (2013).
109. N. Y. Yu *et al.*, Sequence analysis PSORTb 3.0: improved protein subcellular localization prediction with refined localization subcategories and predictive capabilities for all prokaryotes. *Bioinformatics* **26**, 1608–1615 (2010).
110. C. McMahon *et al.*, Yeast surface display platform for rapid discovery of conformationally selective nanobodies. *Nat. Struct. Mol. Biol.* **25**, 289–296 (2018).
111. N. R. Bennett *et al.*, Atomically accurate de novo design of single-domain antibodies. bioRxiv [Preprint] (2024), 10.1101/2024.03.14.585103 (Accessed 26 June 2024).
112. M. A. Rangel *et al.*, Fragment-based computational design of antibodies targeting structured epitopes. *Sci. Adv.* **8**, 9540 (2022).
113. A. Ramon *et al.*, Assessing antibody and nanobody nativeness for hit selection and humanization with AbNatiV. *Nat. Mach. Intell.* **6**, **74**–91 (2024).
114. S. Y. Ting *et al.*, Targeted depletion of bacteria from mixed populations by programmable adhesion with antagonistic competitor cells. *Cell Host Microbe* **28**, 313–321.e6 (2020).
115. B. Jana, K. Keppel, D. Salomon, Engineering a customizable antibacterial T6SS-based platform in *Vibrio natriegens*. *EMBO Rep.* **22**, e53681 (2021).
116. N. H. Le, V. Pinedo, J. Lopez, F. Cava, M. F. Feldman, Killing of Gram-negative and Gram-positive bacteria by a bifunctional cell wall-targeting T6SS effector. *Proc. Natl. Acad. Sci. U.S.A.* **118**, e2106555118 (2021).
117. J. Kreitz *et al.*, Programmable protein delivery with a bacterial contractile injection system. *Nature* **616**, 357–364 (2023).
118. S. J. Hersch, L. Lam, T. G. Dong, Engineered type six secretion systems deliver active exogenous effectors and Cre recombinase. *MBio* **12**, e01115-21 (2021).
119. S. Coulthurst, The type VI secretion system: A versatile bacterial weapon. *Microbiology (United Kingdom)* **165**, 503–515 (2019).
120. J. C. Wohlfarth, D. Ward, J. Pereira, M. Basler, The type VI secretion system and associated effector proteins. *Nat. Rev. Microbiol.* **2025**, 1–16 (2025), 10.1038/s41579-025-01256-w.
121. A. P. West *et al.*, TLR signalling augments macrophage bactericidal activity through mitochondrial ROS. *Nature* **472**, 476–480 (2011).
122. W. P. J. Smith *et al.*, Multiplicity of type 6 secretion system toxins limits the evolution of resistance. *Proc. Natl. Acad. Sci. U.S.A.* **122**, e2416700122 (2025).
123. M. J. Giacalone *et al.*, The use of bacterial minicells to transfer plasmid DNA to eukaryotic cells. *Cell. Microbiol.* **8**, 1624–1633 (2006).
124. M. Jivrajani, N. Shrivastava, M. Nivsarkar, A combination approach for rapid and high yielding purification of bacterial minicells. *J. Microbiol. Methods* **92**, 340–343 (2013).